Journal of Power Sources 243 (2013) 925–934

Contents lists available at SciVerse ScienceDirect

Journal of Power Sources

journal homepage: www.elsevier.com/locate/jpowsour

Investigation of the effects of process sequence on the contact resistance characteristics of coated metallic bipolar plates for polymer electrolyte membrane fuel cells

Cabir Turan [a,b], Ömer Necati Cora [a,c], Muammer Koç [a,d,*]

[a] NSF I/UCRC Center for Precision Forming (CPF), Richmond, VA, USA
[b] Istanbul Gas Distribution Company (IGDAS), Istanbul, Turkey
[c] Karadeniz Technical University, Trabzon, Turkey
[d] Istanbul Sehir University, Istanbul, Turkey

HIGHLIGHTS

- Effects of process sequence on ICR of bipolar plates were investigated.
- PVD coated SS316L BBPs with two different process sequence, namely formed-then-coated and coated-then-formed, were compared.
- Three different coatings (CrN, ZrN, TiN) at three different thicknesses (0.1, 0.5, 1 μm) were used.
- Coated-then-formed BPPs performed similar or even better than formed-then-coated BPPs.

ARTICLE INFO

Article history:
Received 6 March 2013
Received in revised form
29 May 2013
Accepted 31 May 2013
Available online 20 June 2013

Keywords:
Fuel cells
Metallic bipolar plate
Contact resistance
Coating
Manufacturing
Process sequence

ABSTRACT

In this study, results of an investigation on the effects of manufacturing and coating process sequence on the contact resistance (ICR) of metallic bipolar plates (BPP) for polymer electrolyte membrane fuel cells (PEMFCs) are presented. Firstly, uncoated stainless steel 316L blanks were formed into BPP through hydroforming and stamping processes. Then, these formed BPP samples were coated with three different PVD coatings (CrN, TiN and ZrN) at three different thicknesses (0.1, 0.5 and 1 μm). Secondly, blanks of the same alloy were coated first with the same coatings, thickness and technique; then, they were formed into BPPs of the same shape and dimensions using the manufacturing methods as in the first group. Finally, these two groups of BPP samples were tested for their ICR to reveal the effect of process sequence. ICR tests were also conducted on the BPP plates both before and after exposure to corrosion to disclose the effect of corrosion on ICR. Coated-then-formed BPP samples exhibited similar or even better ICR performance than formed-then-coated BPP samples. Thus, manufacturing of coated blanks can be concluded to be more favorable and worth further investigation in quest of making cost effective BPPs for mass production of PEMFC.

1. Introduction

Due to the increasing concerns about the depletion of fossil fuel resources, global warming and air pollution, fuel cell technologies have received an increasing interest in recent decades, owing to their high efficiency and low emission. Among various types of fuel cells, polymer electrolyte fuel cells (PEMFC) are considered as promising candidates for next generation power sources in transportation vehicles and other portable applications. Their advantages include low operating temperature, high power density and easy scale-up. In spite of such benefits, high cost and low durability of PEMFC stacks postpone their widespread commercialization [1].

Bipolar plates (BPPs) are one of the main components of the PEMFC, and they significantly contribute to the strength, cost, weight and volume of the overall system. U.S. Department of Energy (DOE) established a set of goals on required properties of BPPs as listed in Table 1 [2]. Variety of materials has been proposed for BPPs, however; thus far, no material meets all the requirements concurrently [3–9]. Because of good electrical conductivity, low material cost, well-established manufacturing processes and superior mechanical properties, metallic BPPs have been considered as a promising choice. Various grades of stainless steels have been

* Corresponding author. NSF I/UCRC Center for Precision Forming (CPF), Richmond, VA, USA. Tel.: +1 804 859 0835.
E-mail addresses: cabirturan@yahoo.com (C. Turan), koc.muammer@gmail.com (M. Koç).

0378-7753/$ – see front matter © 2013 Elsevier B.V. All rights reserved.
http://dx.doi.org/10.1016/j.jpowsour.2013.05.182

Table 1
DOE's Performance requirements for PEM fuel cell bipolar plates [2].

Characteristic	Unit	2017 Target
Cost	$/kW	3
Hydrogen permeability (ASTM D1434)	$cm^3\ (cm^2\ s)^{-1}$	$<1.3 \times 10^{-14}$
Corrosion at anode, cathode	$\mu A\ cm^{-2}$	<1
Electrical conductivity	$S\ cm^{-1}$	>100
Contact resistance	$m\Omega\ cm^2$	<20
Flexural strength (ASTM D790-10)	MPa	>25
Forming elongation (ASTM E8M-01)	%	40

Table 2
Chemical composition of SS316L (Browns Metals Co., Rancho Cucamonga, CA, USA).

C	Mn	P	S	Si	Cr	Ni	Mo	Cu	N	Fe
0.021	1.48	0.033	0.001	0.43	16.20	10.03	2.06	0.43	0.04	Bal

put forward as BPP material candidates due to their higher formability and higher corrosion resistance than many other metallic materials. However, corrosive environment of harsh PEMFC working conditions and high interfacial contact resistance (ICR) are the main concerns about stainless steel BPPs [10–29]. Thus, in order to improve corrosion resistance and contact conductivity at reasonable cost, protective coatings on stainless steel BPPs have been extensively studied [16,18,19,30–35].

Physical vapor deposition (PVD) nitrides are widely researched to improve corrosion resistance and contact conductivity of metallic BPPs [36–40]. Several studies reported performance evaluation of different coatings such as TiN Refs. [32–35,41–43], CrN [38,40,44–50] and ZrN [51,52] on stainless steel substrate materials. In previous studies by authors, effect of manufacturing process type and conditions on corrosion and contact resistance CrN, TiN and ZrN coated BPPs were investigated [53,54].

When coated metallic materials are needed for BPP, order of process sequence (coating and forming) would be important. Coating of BPPs after forming would be a reasonable path since one can expect that forming of coated blanks may deteriorate the surface due to possible deformation of coatings with brittle characteristics. On the other hand, forming of pre-coated metallic material can increase manufacturing speed of BPPs, and consequently reduces the cost. "Finish first, fabricate later" is a growing trend in sheet metal manufacturing due to promise of simpler workflows, reduced stock, easier environmental compliance and lower overall costs [55,56]. Although the literature is abundant for investigations on the effect of forming process on coating failures [57–60], to the best knowledge of the authors, there is no dedicated study focusing on the effect of manufacturing processes sequence on ICR behavior of coated metallic BPP. The aim of this study is to understand and disclose the effect of process sequence (e.g., coating before forming vs. coating after forming) on the contact resistance of the coated metallic BPPs.

2. Experimental methodology and conditions

To this aim, in this study, two groups of coated metallic BPPs were investigated in terms of process sequence on ICR between BPPs and gas diffusion layer (GDL) in this study. The first group of samples was 'formed-then-coated' while the second group of 'coated-then-formed' samples was coated as blank sheets; then, formed with the same forming methods (stamping and hydroformed). Three different PVD metal nitride coatings, namely titanium nitride (TiN), chromium nitride (CrN), zirconium nitride (ZrN), at three different coating thicknesses, 0.1, 0.5 and 1 μm, were used as performed by Tanury Industries Co. (Lincoln, RI, USA). Table 2 shows chemical composition of SS316L, used in experiments and Table 3 shows PVD process parameters provided by this supplier.

Two different die geometries were employed to obtain different micro-channel arrays on BPP samples. Forming dies were named according to their channel heights as 250 and 750 μm, throughout the study. Forming parameters were selected as 40 MPa pressure with a pressure rate of 1 MPa s^{-1} in hydroforming and 200 kN force with a punch speed of 1 mm s^{-1} in stamping based on the previous studies of authors [29], in which detailed description of the forming processes employed and test setup used were presented.

Surfaces of bipolar plates were examined using Hitachi SU-70 scanning electron microscope (SEM) fitted with EDAX energy dispersive X-ray spectroscopy system (EDS) and HIROX KH-7700 (HIROX-USA, NJ, USA) digital microscope. Wyko NT1100 optical profiler (Veeco Instruments Inc., Tucson, AZ, USA) was also used for surface roughness measurements.

Interfacial contact resistance (ICR) values between samples and carbon paper GDL (Toray TGP-H 60, Toray Corp., Tokyo, Japan) were measured through the method developed by Wang as reported in Ref. [17]. The detailed information about the methodology and experimental setup were explained in previous publications [6,29]. ICR tests were conducted before and after corrosion tests in order to reveal the effect of PEMFC condition (i.e. corrosive) exposure on ICR values. Potentiodynamic electrochemical corrosion test with O_2 bubbling was chosen to simulate cathodic conditions of PEMFC. Potential range was changed between −1.2 V and 0.8 V with respect to standard hydrogen electrode (SHE) at a 1 mV s^{-1} rate in potentiodynamic experiments. Detailed explanation of the corrosion test procedure can be found in an earlier work [5].

Coated-after-forming samples underwent to ICR test as received whereas coated-before-forming BPP samples were subjected to ultrasonic cleaning in an acetone bath prior to ICR tests. Post corrosion test samples were also cleaned by acetone to remove the acidic solution residue.

Table 3
Coating conditions (provided by Tanury Industries, Lincoln, RI).

Run#	Coating	Thickness (μm)	Temperature (°C)	Deposition time (min)	Deposition current (A)	Bias voltage (V)	Nitrogen flow rate (sccm)	Argon flow rate (sccm)	Pressure (m Torr)
1	TiN	0.1	60	6	450	75	500	800	5
2	TiN	0.5	60	38	450	75	500	800	5
3	TiN	1	60	75	450	75	500	800	5
4	CrN	0.1	60	2	450	75	500	800	5
5	CrN	0.5	60	4	450	75	500	800	5
6	CrN	1	60	8	450	75	500	800	5
7	ZrN	0.1	60	2	450	75	500	800	5
8	ZrN	0.5	60	8	450	75	500	800	5
9	ZrN	1	60	16	450	75	500	800	5

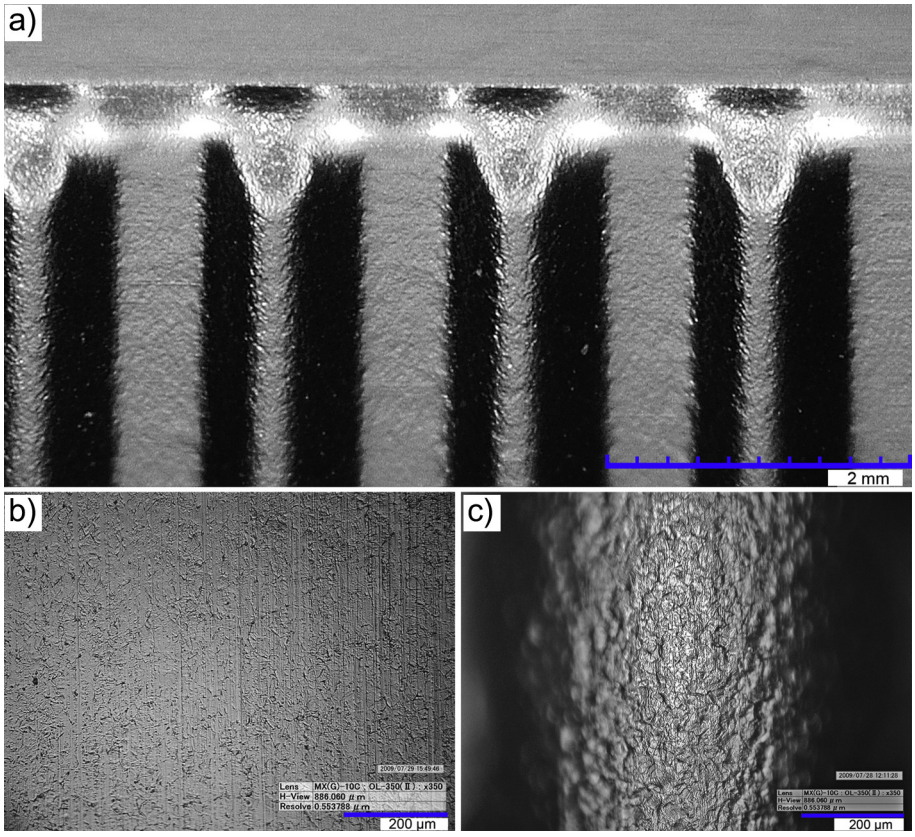

Fig. 1. Digital microscope images for blank and bipolar plate surface a) Image of BPP surface after forming; b) surface morphology of unformed blank; and c) channel tip of BPP.

3. Results and discussions

3.1. Surface evaluation of substrate

Surface morphology of the substrate was examined using confocal optical microscopy. Fig. 1a represents general appearance of formed uncoated BPP surface. Effect of forming process on the surface can easily be seen by comparing unformed blank (Fig. 1b) and channel tip of formed BPP (Fig. 1c). Microscopic surface appearance is presented in Fig. 1.

Surface roughness values of unformed blank and formed BPPs with various surface conditions are reported in Fig. 2. Variation bars in this figure and other hereafter show the range of values recorded during measurements. While roughness values of uncoated and coated BPPs are in same order, roughness of uncoated blank is almost one order of magnitude lower than that of formers.

3.1.1. SEM images of BBP samples

SEM images are used to understand the surface morphology BPP samples. Fig. 3 compares the effect of process sequence on coating structure. The sample in Fig. 3a was formed first, then coated with 1 µm TiN, whereas samples in Fig. 3b, c and d were formed by using pre-coated blanks with 1, 0.5 and 0.1 µm thick TiN layer, respectively. Pitting defects are more visible in formed-then-coated sample (Fig. 3a); coating cracks in transverse direction to strain are clearly noticeable only on coated-then-formed samples. Macro

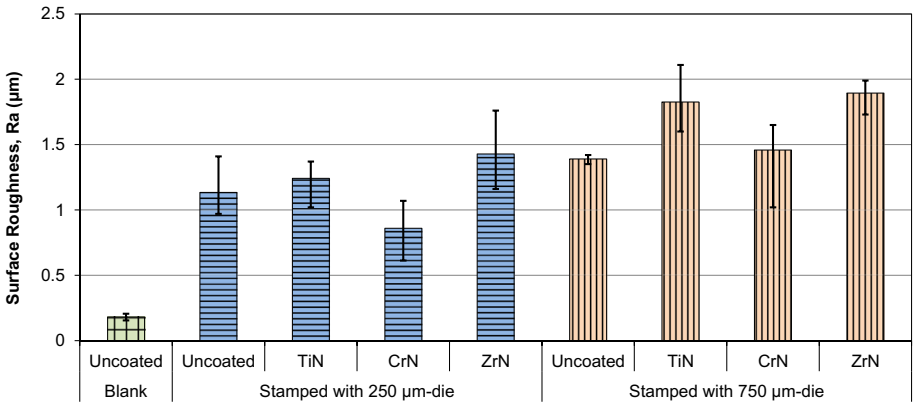

Fig. 2. Surface roughness values of unformed blank substrate and BPP samples with different surface conditions.

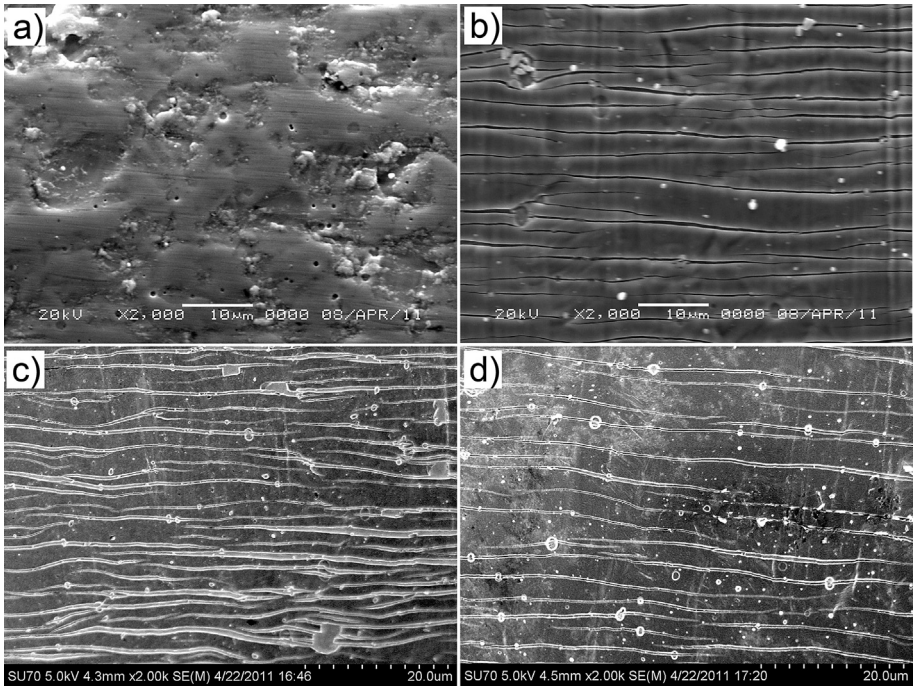

Fig. 3. SEM images for a) 1 μm TiN coated after forming, b) 1 μm, c) 0.5 μm, d) 0.1 μm TiN coated before forming BPP samples.

defects (white particles in pictures) are common for all samples. Density of cracks was higher at channel tips and walls compared to channel valleys due to different deformation pattern, as shown in Fig. 4. Small amount of coating delamination and spallation were also detected as presented. Crack paths mostly overlapped macro defects. This fact can indicate that macro defects behave as notches in coating structure. TiN and ZrN coatings with different thicknesses exhibited similar patterns, mostly directional cracks to perpendicular to strain while various thickness CrN coatings showed different shape of cracks (see Fig. 5). Approximate interval between adjacent cracks was 2 μm for TiN and ZrN coatings regardless of thickness. On the other hand, 0.7 μm crack distance on 1 μm CrN coating reduced to 0.15 μm for 0.1 μm thick CrN coating, roughly. Another difference for 0.1 μm CrN coating was small rhombic cracks instead of directional and continuous patterns compare to others (see Fig. 5).

In order to reveal surface elemental composition differences between non-cracked and coating-cracked area, EDX analysis with accelerating voltage of 25 kV was conducted on 1 μm-thick ZrN coated samples as can be seen in Fig. 6. Analyses revealed substantial differences in ZrN content between areas of interest verifying the coating failure in lower ZrN content zone. Defect-free coating application is assumed to be crucial to maintain corrosion protection in active-surface area while coating cracks, pittings etc. may not be as critical as in corrosion case if those are not in contacting regions of bipolar plates.

Erikkson et al. conducted a similar experiment to investigate the effect of plastic deformation on integrity of TiN coating [60]. They observed that cracking behavior depended on amount of strain and coating thickness. The authors also reported improvement of corrosion resistance of TiN coated samples compared to bare substrate material, in spite of damages on coating layer.

3.1.2. Contact area measurements

Contacting surface area between BPP samples and GDL were measured by placing pressure sensitive film at two side of BPP in compression test. Image J software was used to calculate imprinted areas on in-scale photographs of pressure films (see Fig. 7). Contact area change by compaction pressure is shown in Fig. 8. Contact areas increased with increasing compaction pressure due to deformation of GDL and BPP. Initial rapid increase of contact area became stabilized with the increase of compaction force most likely due to compaction of fibers in GDL.

3.1.3. ICR evolution of BPP samples with compaction pressure

Evolution of the ICR with increasing compaction pressure is presented in Fig. 9 for some of the representative uncoated and coated BPP samples based on total active area of 16 cm^2 on samples.

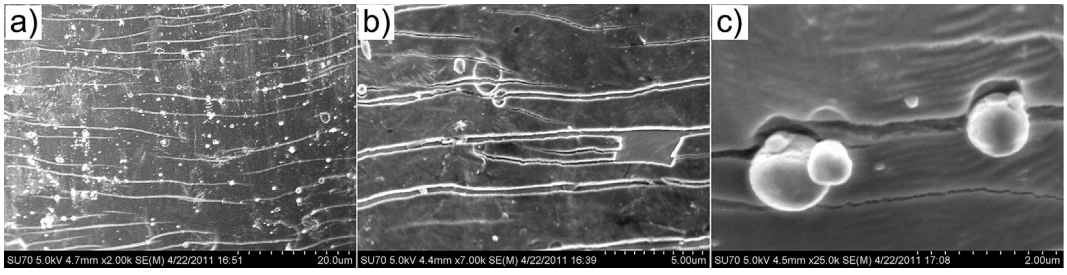

Fig. 4. SEM images of 0.5 μm TiN coated BPP samples showing a) channel valley; b) close-up view cracking and spallation area; and c) macro defects.

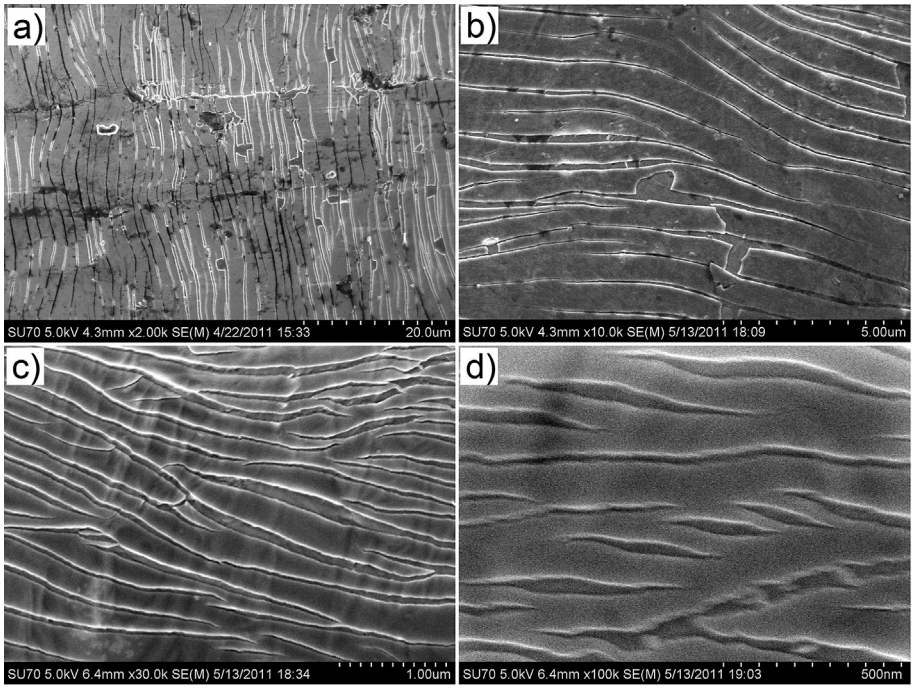

Fig. 5. SEM images of a) 1 μm ZrN; b) 1 μm CrN; c) 0.5 CrN; and d) 0.1 μm CrN coated samples. (All samples were stamped with 750 μm-die and images were taken from channel tips).

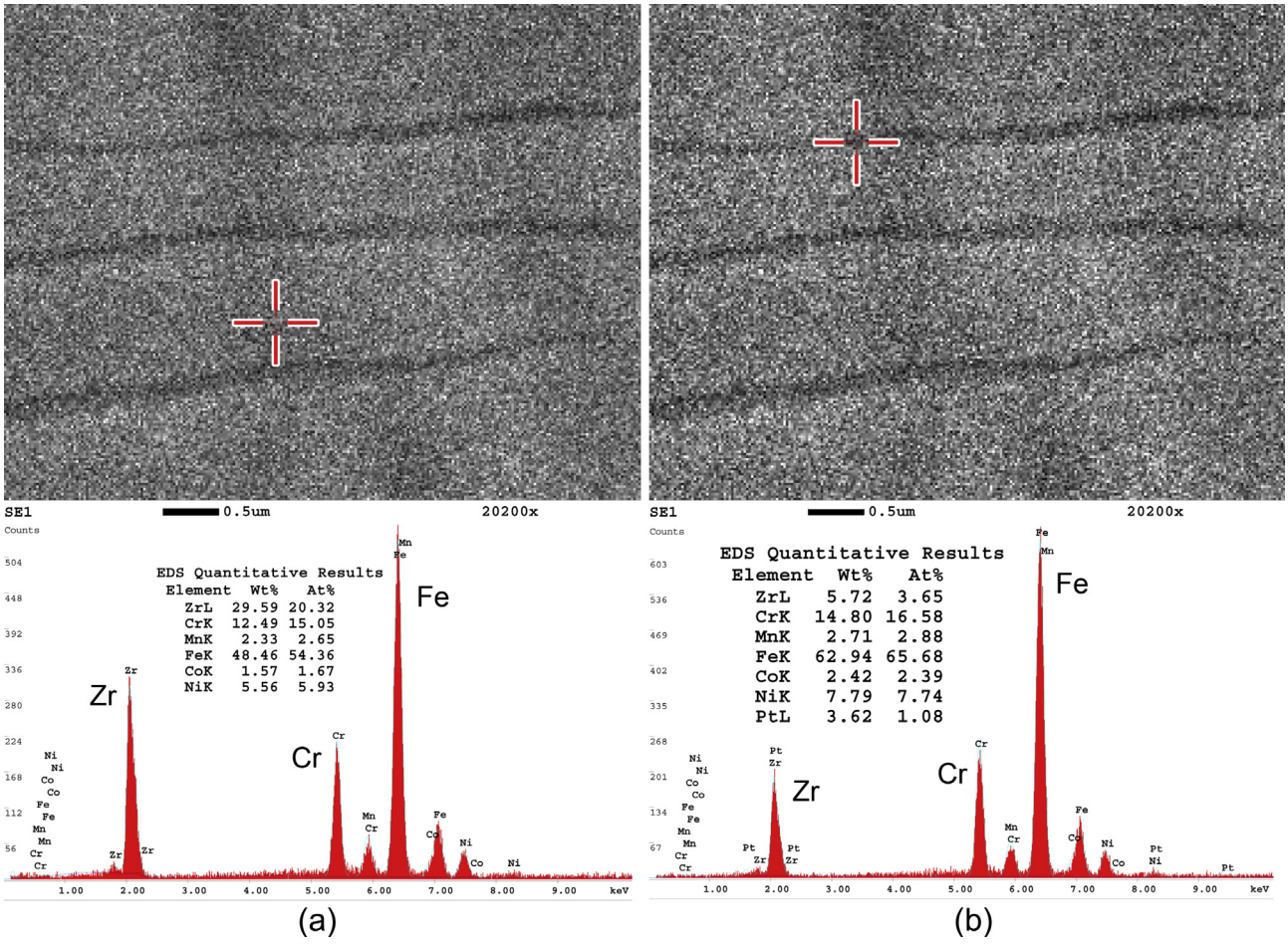

Fig. 6. EDX analyses of ZrN coated BPP samples from a) non-cracked and b) cracked area.

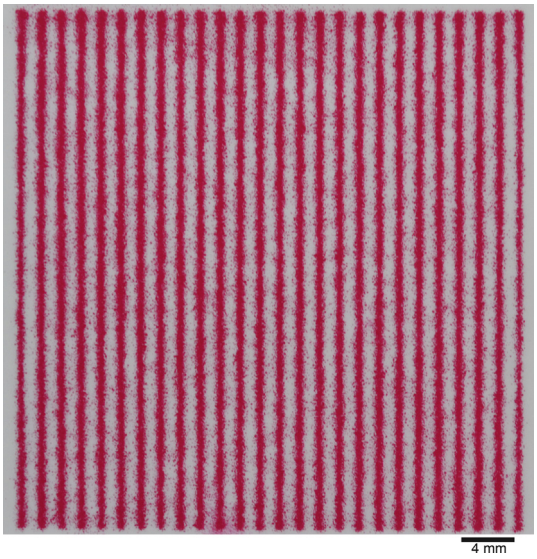

Fig. 7. Determination of contacting surface area between BPP and GDL during ICR test through pressure sensitive film use.

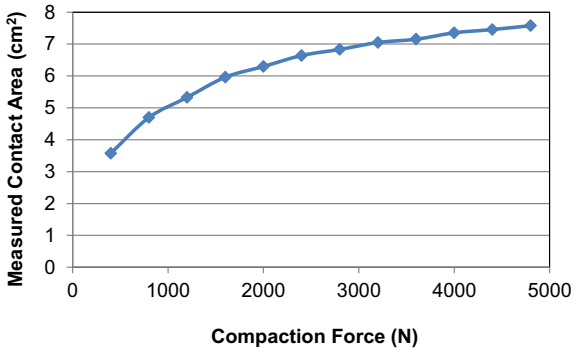

Fig. 8. Contact area change by compaction pressure.

Uncoated BPP sample was also included in the experiments for comparison purposes. Logarithmic scale was used to cover wide range of ICR values of coated samples in the same graph. Variation bars represent maximum and minimum ICR values measured. Due to the increasing real contact area between GDL and BPP surfaces, an exponential decrease in ICR was observed with increasing compaction pressure, as expected. TiN coated samples exhibited the lowest level of contact resistance among the investigated cases, followed by ZrN and CrN coated samples, respectively. ICR performances of uncoated samples were between ZrN and CrN coated samples. While the process sequence (formed + coated vs. coated + formed) did not affect the ICR values in TiN and ZrN cases, significant differences were observed in CrN cases.

ICR and compaction pressure were calculated based on measured contact area, as explained in the previous section, is given in Fig. 10. Ranking of ICR values for the samples did not change; however, ICR and compaction pressure values were shifted for all samples. Due to lack of precision on contact area calculation, ICR values reported were based on total active area of 16 cm^2 hereafter.

3.1.4. *Effect of process sequence on ICR before corrosion test*

BPP samples manufactured with two different process sequences, namely formed + coated and coated + formed, are compared from ICR performance point of view in Fig. 11. CrN coated + formed BPP samples exhibited lower ICR values for all conditions (regardless of forming method, die channel heights and coating thicknesses) than that of formed + coated BPP samples. ANOVA analyses (with 95% confidence interval) indicated that differences between these groups are statistically significant except four cases. (Symbol "*" in Figs. 11–13 indicates that difference between two adjacent column statistically significant). Three out of four cases, in which insignificant changes were observed, are 0.1 μm CrN coated samples. ICR differences between BPP were found to be more distinct at 1 μm coating thickness. One of the most notable differences between these two groups is that the formed +1 μm CrN coated forming showed distinctly higher ICR values than 0.1 and 0.5 μm coating thickness cases whereas this difference was not so distinct for formed + coated BPP samples. This fact can be attributed to the possibility that semiconducting CrN layers fractured during forming process and permitted more electrons to flow in coated + formed cases. ICR values for all CrN coated samples were found to be remarkably higher than the acceptable levels although they were reported as the most corrosion resistant among others [53].

The formed +1 μm TiN coated BPP samples had the best ICR performance among all the tested cases showing contact resistance values smaller than 10 mΩ cm^2, which is DOE contact resistance target for BPPs. Differences between two sequences were significant for all 1 μm cases whereas only one case was found significantly different among 0.1 and 0.5 μm TiN coated cases. In stamping, the

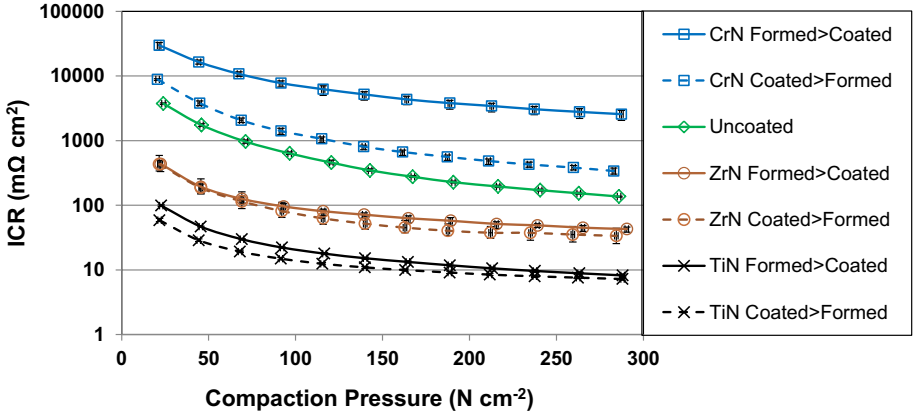

Fig. 9. ICR evolution of BPP samples manufactured with two different sequence as function of compaction pressure based on total active area of 16 cm^2 [(Coating thickness: 1 μm, Forming Method: Stamping, Die: 750 μm channel height).

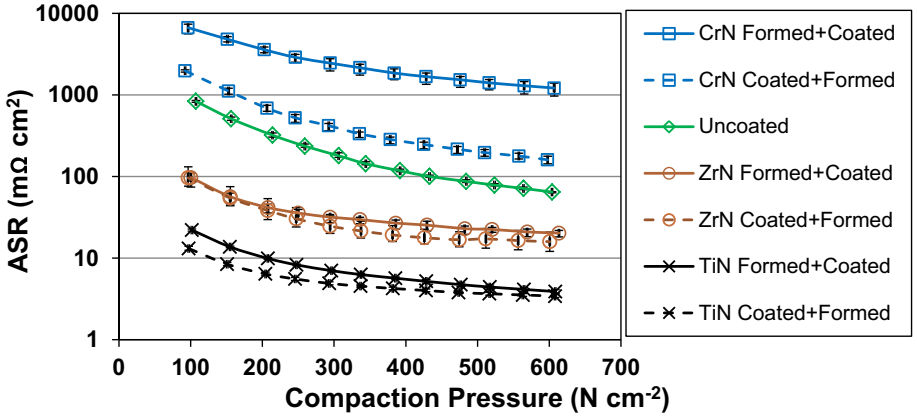

Fig. 10. ICR evolution of BPP samples manufactured with two different sequence as function of compaction pressure based on contact area measured pressure sensitive film. (Coating thickness: 1 μm, Forming method: stamping, Die: 750 μm channel height).

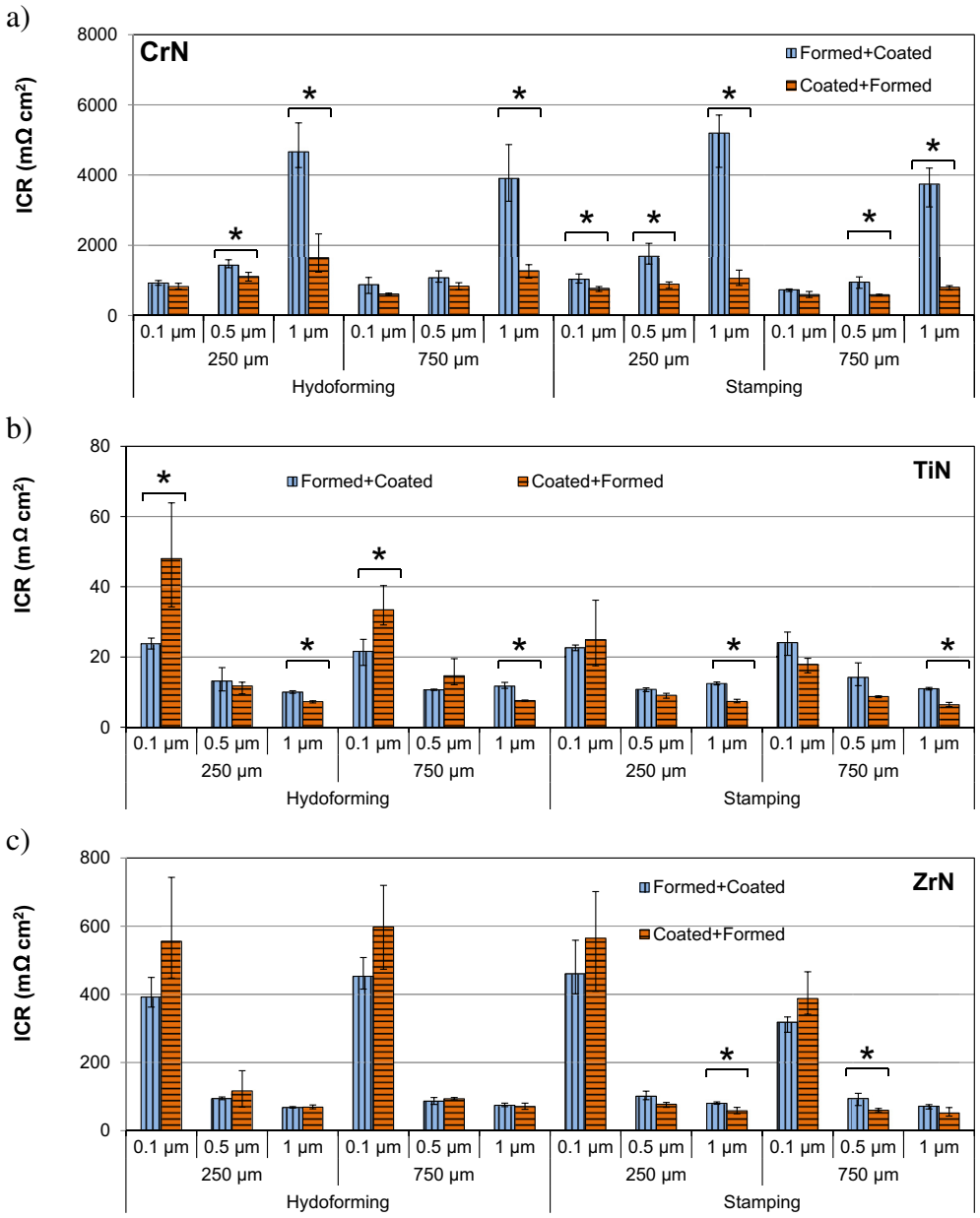

Fig. 11. ICR of a) CrN, b) TiN, c) ZrN coated BPP samples at 140 N cm^{-2} (for hydroforming and stamping; using 250 and 750 μm feature sized dies; and 0.1, 0.5 and 1 μm coating thicknesses). * Indicates statistically significant difference between two adjacent columns.

effect of process sequence was found to be insignificant for ZrN coated samples, in general (except two out of 12 cases). 0.5 and 1 μm coated ZrN samples had similar ICR behavior while 0.1 μm coated samples showed markedly higher ICR compared to them. Although 0.5 and 1 μm thick ZrN coating significantly improved ICR behavior of BPP samples compared to bare substrate of SS316L, their ICR values (minimum value of 52 mΩ cm^2) were significantly higher than the target value of 10 mΩ cm^2.

Alaca et al. tested effect of tensile strain on resistivity for aluminum thin films (400 nm) on 152 μm-thick polyimide substrates [61]. They reported steep increase in resistivity by strain due to micro-crack formation on aluminum film. A similar study with 100 nm thick aluminum films on micrometer-thick polysulfone was reported by Bautista et al., recently [62]. They observed a slight decrease on resistivity at the beginning of the tensile test and then similar increase in resistivity with increasing strain due to cracks occurred on the film. Although such studies provide information on conductive films on insulating substrate (typical for electronic and electro-mechanic applications), the relevance of this information to present study is very limited due to different nature of the application. Interest was on "through plane electron flow" in this study whereas cited studies investigated "in plane current" mainly.

3.1.5. Effect of corrosion exposure on ICR

Effect of corrosion test on ICR values of BBP samples, which are coated before and after forming, is also compared. As depicted in Fig. 12, ICR values of CrN coated BPP samples significantly decreased only in two cases whereas changes for the remaining 10 cases were found to be insignificant. All the ICR values for TiN coated samples increased after corrosion test. Although these increases are noticeable, approximately three-fold for 0.1 μm, two-fold for 0.5 μm and 20% for 1 μm coating thicknesses, ANOVA showed that changes were only statistically significant for half of the cases due to scattered ICR values obtained after corrosion test. Similar to TiN coated BPP samples, ICR of ZrN coated samples increased after corrosion test, as well. However, ICR differences between before and after corrosion tests were not distinct, opposed to TiN coated samples as ANOVA revealed statistically significant increases in three out of twelve case, only. Decrease in ICR of CrN coated samples can be ascribed to the fact that degradation of

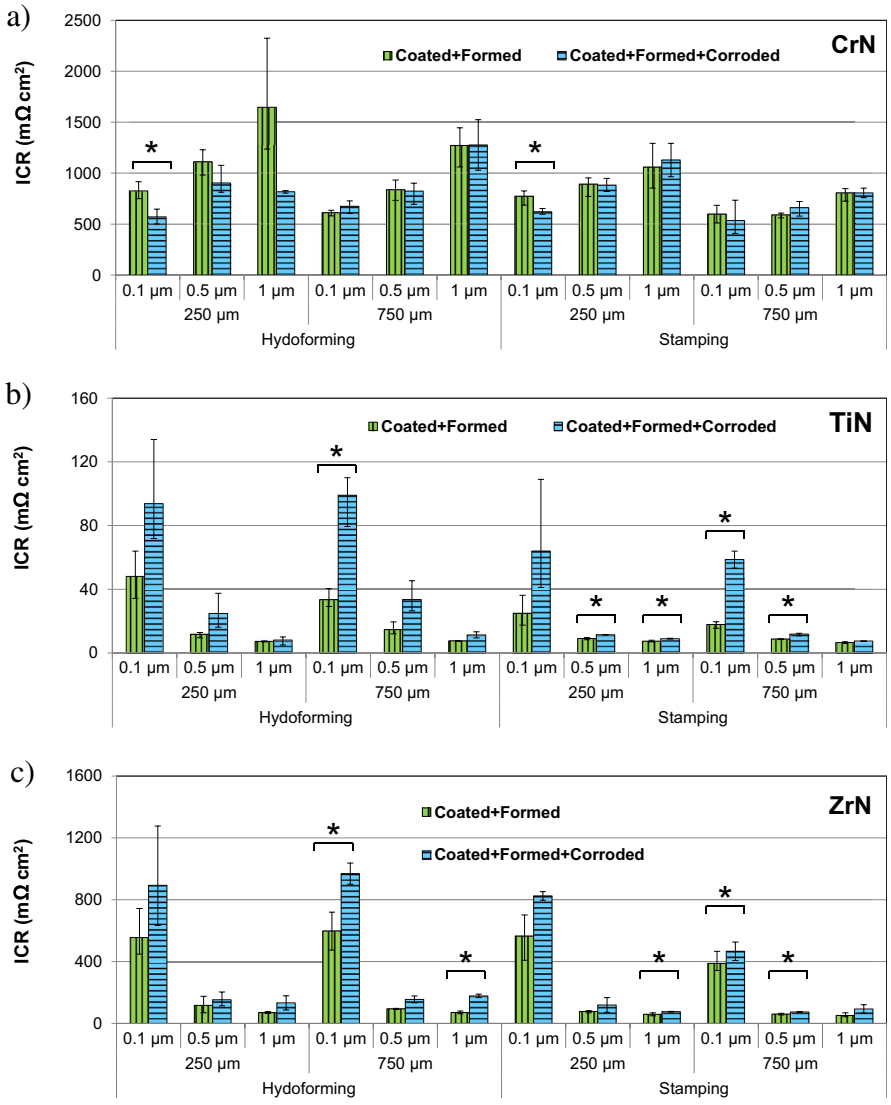

Fig. 12. ICR values of a) CrN, b) TiN, c) ZrN coated BPP samples at 140 N cm^{-2} before and after corrosion test. (Hydroforming and stamping are two forming methods; 250 and 750 μm are two die channel heights; 0.1, 0.5 and 1 μm are coating thicknesses).

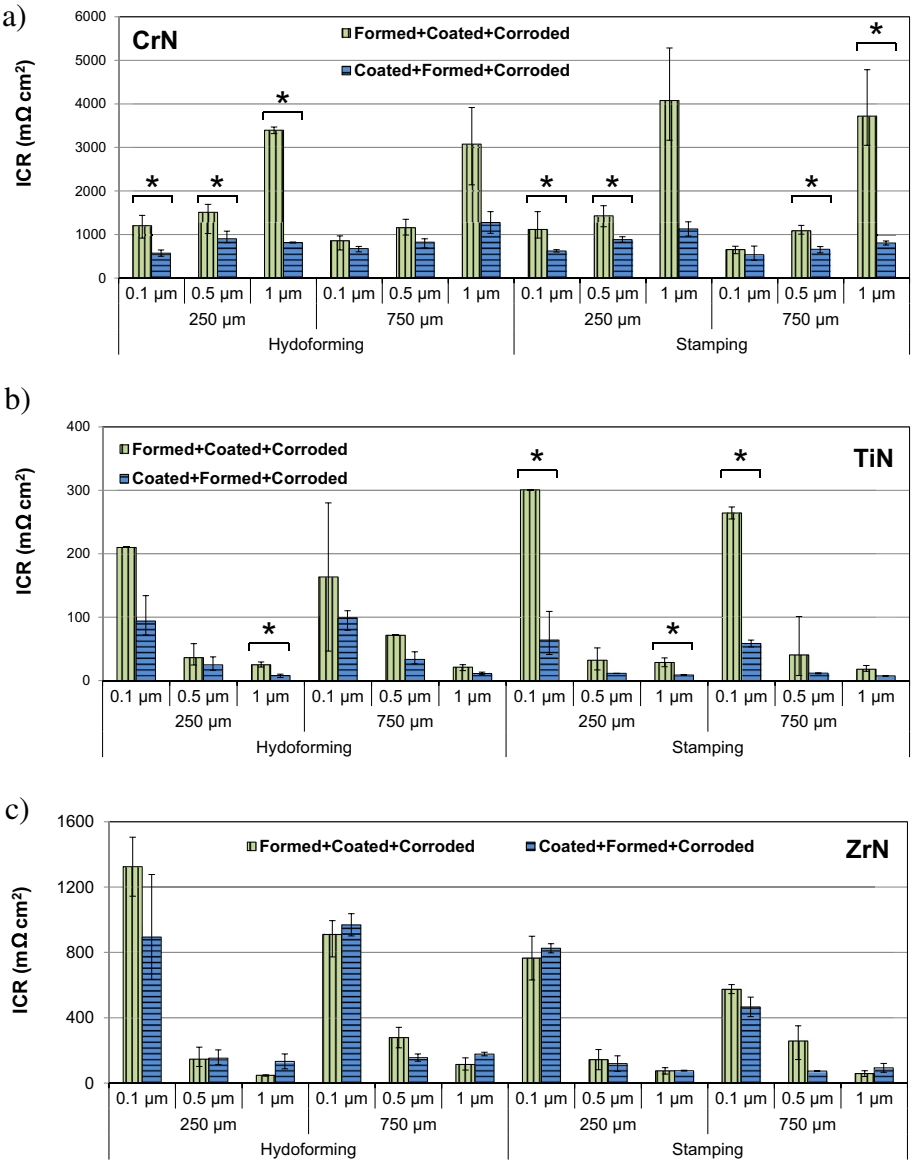

Fig. 13. ICR values of a) CrN, b) TiN, c) ZrN coated BPP samples manufactured with two different sequences after corrosion test at 140 N cm^{-2} (for hydroforming and stamping; using 250 and 750 μm feature sized dies; and 0.1, 0.5 and 1 μm coating thicknesses).

semiconducting CrN layer increased the conductivity yet CrN coated BPPs had higher ICR values than that of uncoated samples.

3.1.6. *Effect of process sequence on ICR after corrosion exposure*

BPP samples manufactured with two different process sequences were compared after they were exposed to 30 min PD corrosion tests. As a general remark, corrosion resistance of coatings were in descending order of ZrN > CrN > TiN, similar to a recent study result [53]. ICR tests after corrosion exposure revealed that formed + CrN coated samples showed lower ICR compared to CrN coated BPP samples after forming. In most cases, difference between these two groups of samples was found to be statistically significant. Similar to CrN coated samples, TiN coated + formed BPP samples demonstrated lower ICR values compared to other forming sequence. In four out of twelve cases, statistically significant differences were detected through ANOVA because of scattered ICR values. In the case of ZrN coated samples, different forming sequence did not result in any clear pattern on ICR. In addition, differences between these two groups (coated + formed vs. formed + coated) were found to be statistically insignificant. More stable ICR performance of ZrN coated samples after corrosion test can be attributed to the better corrosion resistance of ZrN compared to CrN and TiN.

3.2. *Conclusion*

The effect of process sequence on ICR values of CrN, TiN and ZrN coated SS316L BPPs was investigated. Coating of bipolar plate samples before or after forming process altered the ICR behavior of the metallic bipolar plate samples. In CrN coating case, coating before forming resulted in lower ICR compared to the reverse order, coating after forming. Nevertheless, all the ICR values acquired for the CrN coated samples were extremely higher than the required level of BPP materials. TiN coated samples exhibited the best ICR performance in current study meeting DOE targets. ICR values of formed-then-coated BPP samples were recorded smaller than that for coated-then-formed BPPs. The downside of TiN coated samples was their vulnerability to corrosion exposure. ICR values of TiN

coated samples were observed to significantly increase after exposure to corrosion. ZrN coated samples showed an improved ICR performance compared to bare SS316L samples, as expected, and desired from coating application. Nevertheless, their ICR values were not low enough to meet the DOE target. Process sequence was not significantly effective on ICR behavior of ZrN coated plates in both before and after corrosion test. A vital advantage of ZrN coating was that ZrN coated samples showed similar ICR performance after and before exposure to corrosion conditions. In summary, metallic coated-then-formed BPP samples exhibited similar even, in some cases, better performance than formed-then-coated BPP samples in terms of ICR. Thus, it can be concluded that continuous coating of unformed strips prior to forming of BPP samples seemed to be favorable and worth more detailed investigations to realize the cost effective BPP manufacturing for PEMFC applications.

References

[1] Y. Wang, K.S. Chen, J. Mishler, S.C. Cho, X.C. Adroher, Appl. Energy 88 (2011) 981–1007.
[2] United States Department of Energy- Energy Efficiency and Renewable Energy, Fuel Cell Technologies Program, 2011 Technical Plan – Fuel Cells, Web site: http://www1.eere.energy.gov/hydrogenandfuelcells/mypp/pdfs/fuel_cells.pdf (Last accessed at 05.19.2013).
[3] S. Mahabunphachai, Ö.N. Cora, M. Koç, J. Power Sources 195 (2010) 5269–5277.
[4] F. Dundar, E. Dur, S. Mahabunphachai, M. Koç, J. Power Sources 195 (2010) 3546–3552.
[5] E. Dur, Ö.N. Cora, M. Koç, J. Power Sources 196 (2011) 1235–1241.
[6] C. Turan, E. Dur, M.F. Peker, O.N. Cora, M. Koc, Corrosion, contact resistance, and surface characteristics of stamped and hydroformed metallic bipolar plates for PEMFC, in: Proceedings of FUELCELL2010, the 8th International Conference on Fuel Cell Science, Engineering and Technology, June 14–16, 2010, Brooklyn, New York, USA (2010), pp. 545–553.
[7] M. Koç, S. Mahabunphachai, J. Power Sources 172 (2007) 725–733.
[8] S. Mahabunphachai, M. Koç, Int. J. Mach. Tools Manu. 48 (2008) 1014–1029.
[9] S. Mahabunphachai, M. Koç, J. Power Sources 175 (2008) 363–371.
[10] V. Mehta, J.S. Cooper, J. Power Sources 114 (2003) 32–53.
[11] J. Wind, R. Späh, W. Kaiser, G. Böhm, J. Power Sources 105 (2002) 256–260.
[12] A.J. Appleby, Energy 21 (1996) 521–653.
[13] A. Hermann, T. Chaudhuri, P. Spagnol, Int. J. Hydrogen Energy 30 (2005) 1297–1302.
[14] H. Tawfik, Y. Hung, D. Mahajan, J. Power Sources 163 (2007) 755–767.
[15] Y. Shao, G. Yin, Z. Wang, Y. Gao, J. Power Sources 167 (2007) 235–242.
[16] N. de las Heras, E.P.L. Roberts, R. Langton, D.R. Hodgson, Energy Environ. Sci. 2 (2009) 206–214.
[17] H. Wang, M.A. Sweikart, J.A. Turner, J. Power Sources 115 (2003) 243–251.
[18] S. Lee, C. Huang, Y. Chen, J. Mater. Process. Technol. 140 (2003) 688–693.
[19] S.J. Lee, C.H. Huang, Y.P. Chen, C.T. Hsu, J. Fuel Cell Sci. Technol. 2 (2005) 290–294.
[20] B. Cunningham, D.G. Baird, J. Mater. Chem. 16 (2006) 4385–4388.
[21] H. Wang, J.A. Turner, J. Power Sources 180 (2008) 791–796.
[22] R. Tian, J. Sun, J. Wang, Int. J. Hydrogen Energy 33 (2008) 7507–7512.
[23] Y. Wang, D.O. Northwood, Adv. Mater. Res. 41 (2008) 469–475.
[24] J. André, L. Antoni, J.P. Petit, Int. J. Hydrogen Energy 35 (2010) 3684–3697.
[25] J. André, L. Antoni, J. Petit, E. De Vito, A. Montani, Int. J. Hydrogen Energy 34 (2009) 3125–3133.
[26] R.A. Antunes, M.C.L. Oliveira, G. Ett, V. Ett, Int. J. Hydrogen Energy 35 (2010) 3632–3647.
[27] P. Hamilton, B. Pollet, Fuel Cells 10 (2010) 489–509.
[28] A. Heinzel, F. Mahlendorf, C. Jansen, Fuel cells – proton-exchange membrane fuel cells bipolar plates, in: Jürgen Garche (Ed.), Encyclopedia of Electrochemical Power Sources, Elsevier, Amsterdam, 2009, pp. 810–816.
[29] C. Turan, Ö.N. Cora, M. Koç, Int. J. Hydrogen Energy 36 (2011) 12370–12380.
[30] T. Fukutsuka, T. Yamaguchi, S. Miyano, Y. Matsuo, Y. Sugie, Z. Ogumi, J. Power Sources 174 (2007) 199–205.
[31] Y. Show, Surf. Coat. Technol. 202 (2007) 1252–1255.
[32] M. Li, S. Luo, C. Zeng, J. Shen, H. Lin, C. Cao, Corros. Sci. 46 (2004) 1369–1380.
[33] Y. Wang, D.O. Northwood, J. Power Sources 165 (2007) 293–298.
[34] Y. Wang, D.O. Northwood, Int. J. Hydrogen Energy 32 (2007) 895–902.
[35] E.A. Cho, U.S. Jeon, S. Hong, I.H. Oh, S.G. Kang, J. Power Sources 142 (2005) 177–183.
[36] R. Tian, J. Sun, L. Wang, Int. J. Hydrogen Energy 31 (2006) 1874–1878.
[37] H. Lee, S. Lee, J. Kim, M. Kim, D. Wee, Int. J. Hydrogen Energy 33 (2008) 4171–4177.
[38] H. Wang, M.P. Brady, G. Teeter, J. Turner, J. Power Sources 138 (2004) 86–93.
[39] Y. Wang, D.O. Northwood, Electrochim. Acta 52 (2007) 6793–6798.
[40] H. Wang, M.P. Brady, K.L. More, H.M. Meyer III, J.A. Turner, J. Power Sources 138 (2004) 79–85.
[41] L. Ma, S. Warthesen, D. Shores, J. New Mater. Electrochem. Syst. 3 (2000) 221–228.
[42] P.L. Hentall, J.B. Lakeman, G.O. Mepsted, P.L. Adcock, J.M. Moore, J. Power Sources 80 (1999) 235–241.
[43] M. Kumagai, S. Myung, R. Asaishi, Y. Sun, H. Yashiro, Electrochim. Acta 54 (2008) 574–581.
[44] M.P. Brady, K. Weisbrod, C. Zawodzinski, I. Paulauskas, R.A. Buchanan, L.R. Walker, Electrochem. Solid-State Lett. 5 (2002) A245–A247.
[45] I.E. Paulauskas, M.P. Brady, H.M. Meyer III, R.A. Buchanan, L.R. Walker, Corros. Sci. 48 (2006) 3157–3171.
[46] M. Brady, B. Yang, H. Wang, J. Turner, K. More, M. Wilson, F. Garzon, JOM 58 (2006) 50–57.
[47] R. Silva, A. Pozio, J. Fuel Cell Sci. Technol. 4 (2007) 116–122.
[48] R.F. Silva, D. Franchi, A. Leone, L. Pilloni, A. Masci, A. Pozio, Electrochim. Acta 51 (2006) 3592–3598.
[49] A. Pozio, R.F. Silva, A. Masci, Int. J. Hydrogen Energy 33 (2008) 5697–5702.
[50] N.D. Nam, J.G. Kim, Jpn. J. Appl. Phys. 47 (2008) 6887–6890.
[51] W. Yoon, X. Huang, P. Fazzino, K.L. Reifsnider, M.A. Akkaoui, J. Power Sources 179 (2008) 265–273.
[52] J. Barranco, F. Barreras, A. Lozano, A.M. Lopez, V. Roda, J. Martin, M. Maza, G.G. Fuentes, E. Almandoz, Int. J. Hydrogen Energy 35 (2010) 11489–11498.
[53] E. Dur, Ö.N. Cora, M. Koç, Int. J. Hydrogen Energy 36 (2011) 7162–7173.
[54] C. Turan, Ö.N. Cora, M. Koç, Int. J. Hydrogen Energy 37 (2012) 18187–18204.
[55] M. Sachtleber, D. Raabe, H. Weiland, J. Mater. Process. Technol. 148 (2004) 68–76.
[56] E. Reinhold, J. Richter, U. Seyfert, C. Steuer, Surf. Coat. Technol. 188-189 (2004) 708–713.
[57] E. Bemporad, M. Sebastiani, C. Pecchio, S. De Rossi, Surf. Coat. Technol. 201 (2006) 2155–2165.
[58] T. Ganne, J. Crépin, S. Serror, A. Zaoui, Acta Mater. 50 (2002) 4149–4163.
[59] V. Teixeira, Thin Solid Films 392 (2001) 276–281.
[60] L. Eriksson, E. Harju, A.S. Korhonen, K. Pischow, Surf. Coat. Technol. 53 (1992) 153–160.
[61] E.B. Alaca, M.T.A. Saif, H. Sehitoglu, Acta Mater. 50 (2002) 1197–1209.
[62] J.R. Bautista, F. Avilés, A.I. Oliva, O. Ceh, J.E. Corona, Mater. Charact. 61 (2010) 325–329.